Comparison of measurement methods of the front velocity of small-scale debris flows

Comparison of measurement methods of the front velocity of small-scale debris flows

Francesco Bettella,[1] Gian Battista Bischetti,[2] Vincenzo D'Agostino,[1] Simone Virginio Marai,[2] Enrico Ferrari,[2] Tamara Michelini[1]

[1]Department of Land, Environment, Agriculture and Forestry, University of Padova, Legnaro (PD); [2]Department of Agricultural and Environmental Sciences - Production, Landscape, and Agroenergy, University of Milan, Italy

Abstract

Debris flow is a gravity-driven process, which is characterized by a travelling dense surge including large boulders, and it is followed by a more fluid tail. These characteristics make difficult the measurement of the mean flow velocity by means of common hydraulic techniques. Different methods can be used at real scale and small-scale to measure the front velocity but a dedicate comparison between available methods is still lacking. This research aims to compare the front velocity measurements in the transport zone of a miniature debris flow using three devices: i) a common digital video camera (29 frames per second); ii) a high speed thermo camera (60 fps); and iii) a laser photoelectric sensors system. The statistical analysis of data has highlighted no significant differences exist between front velocities obtained by means of the video camera and the thermo camera, whereas photocells data statistically differ from those achieved via the other systems. Some lack of data recorded by photocell was documented, while the thermo camera technique did not show significant loss of information being also helpful to detect the kinematic behaviour of single particles. Finally, the tests confirmed the influence of the solid volumetric concentration in the debris-flow mechanics, which promotes, *ceteris paribus*, the debris-flow slowing down.

Correspondence: Francesco Bettella, Department of Land, Environment, Agriculture and Forestry, University of Padova, viale dell'Università 16, 35020 Legnaro (PD), Italy.
Tel.: +39.049.8272700 - Fax: +39.049.8272686.
E-mail: francesco.bettella@unipd.it

Key words: Debris-flow velocity; flume experiments; laser photoelectric sensors; small-scale model; thermo camera.

Acknowledgments: the research was granted by Junior Research Grant 2013, CPDR138494 (University of Padova, Prof. Vincenzo D'Agostino).

Received for publication: 15 May 2015.
Accepted for publication: 14 August 2015.

Journal of Agricultural Engineering 2015; XLVI:472
doi:10.4081/jae.2015.472

Introduction

Several hydraulic methods exist to measure the flow velocity: current meters, weirs, Venturi flumes, Parshall flumes, chemical tracers, *etc*. (Chow, 1959). Debris flow is a geomorphological process characterized by a water-sediment front that can contain large boulders. Moreover, its physical properties, such as density, flow velocity, and shear rate, change in time and in space, making difficult the use of point measurements. For these reasons, the front velocity cannot be easily measured through the common hydraulic techniques (Arattano and Marchi, 2005). At real scale, the continuous measurements of surface velocity are possible using spatial filter velocimetry, electromagnetic Doppler speedometers (Itakura *et al.*, 1985; Itakura and Suwa, 1989; Suwa *et al.*, 1993; Inaba *et al.*, 1997) and image processing techniques (Arattano and Marchi, 2000; Prochaska *et al.*, 2008). Measurements of the mean front velocity are possible with ultrasonic (Pierson, 1986; Arattano *et al.*, 1997), seismic and acoustic sensors (Itakura *et al.*, 1997; Arattano and Moia, 1999). In laboratory, different methods were used in full-scale and small-scale experiments to measure front velocity, but their direct comparison is still lacking. Iverson *et al.* (2010) tracked flow-front of water sediment mixtures with still-frame cameras and video cameras. D'Agostino *et al.* (2013) determined front velocity on a horizontal plane using a high-speed camera and comparing two successive frames. Hürlimann *et al.* (2015) measured travel time using laser devices. Recently, Larcher *et al.* (2007) applying the particle tracking velocimetry (PTV) developed a digital imaging approach, based on Voronoï imaging methods, to study the kinematic of high concentration granular-liquid mixtures using PVC pellets. Similarly, Tuyen and Cheng (2012) combining the PTV and the particle image velocimetry (PIV) techniques analysed the bed load transport of large spherical particles.

This research focuses on the comparison between different methods to measure debris-flow front velocities in laboratory experiments. A total of 29 runs were performed assessing the front velocity by means of three types of devices: i) video camera; ii) thermo camera; and iii) laser photoelectric sensors. The use of thermo camera to apply the PIV and PTV techniques represents an innovative method in small-scale debris flow simulation. In fact, thermo camera is able to track preheated particles during the entire process, also when they are covered by the fluid matrix. A statistical analysis was then performed to verify the differences between the different approaches. Last considerations entail the role of sediment concentration of the debris-flow mixture in affecting, *ceteris paribus*, the surge velocity.

Materials and methods

The laboratory tests were conducted in a small-scale flume at the

Department of Agricultural and Environmental Sciences - Production, Landscape, and Agroenergy of the University of Milan. The laboratory flume measures 2 m in length, 0.15 m in width, and 0.40 m in height, and can be set at angles in a range from 15° to 45°. The experiments were carried out adopting a flume slope angle of 20°. A gate was fixed at the upper end of the flume forming a tank for the mixture accumulation. The gate was sealed placing a thin layer of bentonite clay on the gate perimeter. There was a runout area (settable slope from 0° to 10°) at the end of the flume for the observations of the deposits. The bottom of the test flume was made of a metal crosshatched sheet to reproduce the roughness of the channel and the deposition zone.

The experiments were carried out by tilting the channel at the slope angle of 20°, positioning the gate in the flume, pouring a debris-flow mixture in the tank, stirring the mixture to avoid sedimentation, and finally removing the gate to allow a rapid release of the mixture.

The front velocity in the flume was measured using the following systems: i) a timing system based on laser photoelectric sensors detecting the passage of debris-flow front (system similar to those used by Hürlimann *et al.*, 2015); ii) post processing of images (like systems adopted by Iverson *et al.*, 2010, or D'Agostino *et al.*, 2013) collected by two instruments: a low-cost video camera and a professional high-speed thermo camera.

The velocity was assessed as mean travel velocity of the front in four different reference cross sections (P_i, Figure 1) of the flume. The velocities (V_i) were calculated as ratio of the sub-reach length (R_i, Figure 1) and the time spent to cover the distance. The travel time was measured with a digital time-recorder for the laser photoelectric sensors system, and with the back analysis of the frames for the post processing images systems. A schematic representation of the flume with the location of the four reaches is showed in Figure 1. The position of the photocells above the flume is also illustrated in this figure. Table 1 lists the distances between the gate and the end of each reach where each photocell was located. A description of the measurement instruments under comparison is reported in the following paragraphs.

Experimental debris-flow mixtures

The laboratory tests were performed with mixtures of water and sediment collected from the debris-flow deposits of the Rio Gadria (Eastern Alps, Italy). The debris-flow events that characterize this torrent are described by Comiti *et al.* (2014). The sediment composition of the entrained material presents an important muddy component. The maximum particle diameter used to prepare the debris-flow mixtures under test is equal to 19 mm. This value was chosen to obtain a ratio between the dimension of the biggest particles and the channel width equal to 0.13, which is similar to that observed in the Gadria creek. The sediment sample is sandy loam and its grain size distribution is reported in Figure 2. The sediment was mixed with different amounts of water to obtain mixtures having a total constant volume of 4000 cm^3 and four different solid concentrations by volume C_V (0.50, 0.55, 0.60, and 0.65).

Laser photoelectric sensors system

Five single-beam photocells were installed along the flume. Each photocell was 0.375 m apart. The first photocell (*Start* in Figure 1) was positioned 0.30 m downstream of the gate and it was used to trigger an integrated time-record system. Photocells were installed at a height of 0.30 m above the flume bottom. Photocells transmit the signal of the first interruption of the laser beam to the programmed timer. The device allowed the time recording of the front passage under the photocell. The time was measured with a precision of 0.01 s.

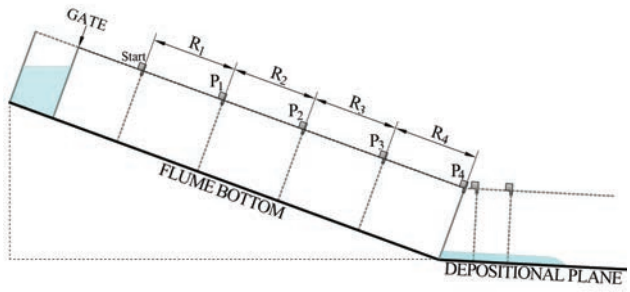

Figure 1. Sketch of the flume (side view) with the position of the four reaches (R_{1-4}) and of the photocells (P_{1-4}) (two photocells were placed over the depositional area but their data were not used).

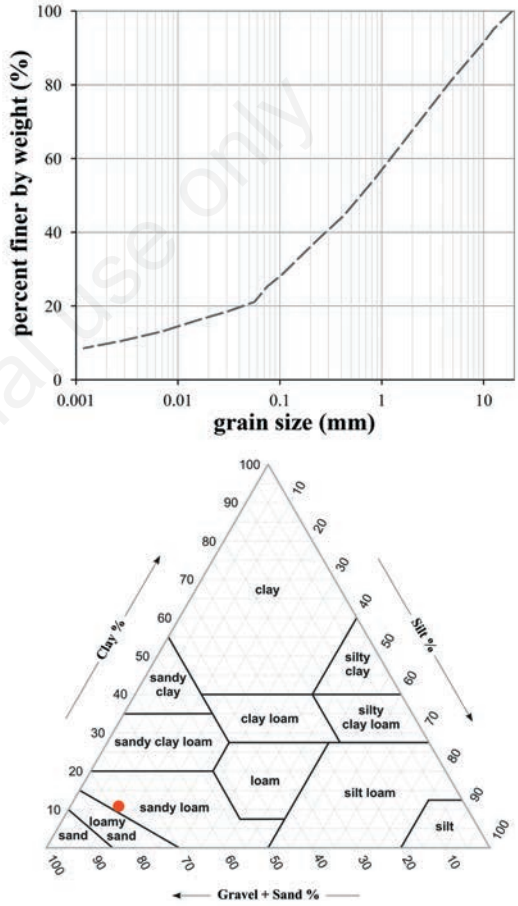

Figure 2. Grain size distribution (above) and corresponding ternary diagram (below) of the sample collected in the Gadria creek and used for the laboratory tests.

Table 1. Distances between the gate of the release tank and the end of the different reaches where a photocell is placed.

Distance from the gate (m)	Photocell	End of the reach
0.300	*Start*	-
0.675	P_1	R_1
1.050	P_2	R_2
1.425	P_3	R_3
1.800	P_4	R_4

Table 2. Data collected for the 29 laboratory tests.

Test ID	C_V	M (kg)	V_O (m^3)	Method of measure	V_1 (m s^{-1})	V_2 (m s^{-1})	V_3 (m s^{-1})	V_4 (m s^{-1})	V_m (m s^{-1})
1	0.50	4.59	0.00253	V	1.55	1.81	2.72	2.18	1.98
				P	-	1.63	2.21	-	1.88
				T	1.41	1.41	2.05	2.25	1.70
2	0.55	4.73	0.00249	V	-	-	-	-	-
				P	2.21	1.39	2.21	1.88	1.85
				T	1.32	1.88	1.41	2.05	1.61
3	0.60	5.79	0.00292	V	1.81	1.36	2.18	1.55	1.67
				P	1.79	1.88	1.44	2.08	1.76
				T	1.41	1.41	1.73	1.32	1.45
4	0.65	5.91	0.00287	V	1.55	0.91	1.81	1.21	1.28
				P	1.34	1.34	1.29	1.07	1.25
				T	1.41	1.18	1.07	1.02	1.15
5	0.50	4.21	0.00232	V	1.55	1.81	2.72	2.18	1.98
				P	-	2.21	1.88	1.88	1.97
				T	1.25	1.41	2.05	1.73	1.55
6	0.55	4.64	0.00245	V	-	-	-	-	-
				P	-	2.34	1.79	2.21	2.08
				T	-	-	-	-	-
7	0.60	5.84	0.00295	V	-	-	-	-	-
				P	1.70	-	1.70	2.50	1.85
				T	1.50	1.50	1.61	1.41	1.50
8	0.65	6.10	0.00296	V	1.36	1.36	1.09	1.36	1.28
				P	-	-	1.39	1.04	1.25
				T	1.73	1.07	1.50	1.18	1.32
9	0.50	5.30	0.00292	V	1.81	1.81	1.81	2.18	1.89
				P	-	1.88	2.21	1.63	1.88
				T	2.25	1.61	2.05	1.88	1.91
10	0.55	5.80	0.00306	V	1.36	1.36	1.81	2.18	1.61
				P	-	1.50	-	-	1.50
				T	1.73	1.25	1.88	2.05	1.67
11	0.60	6.19	0.00313	V	1.36	0.99	1.81	1.55	1.36
				P	1.34	1.01	2.34	1.50	1.42
				T	1.50	0.98	1.88	1.73	1.43
12	0.65	5.93	0.00288	V	1.55	1.09	1.36	1.09	1.24
				P	1.56	1.63	1.10	0.99	1.26
				T	1.61	1.25	1.25	1.18	1.30
13	0.60	5.77	0.00292	V	1.55	1.55	1.81	1.55	1.61
				P	2.21	1.17	1.70	-	1.58
				T	-	-	-	-	-
14	0.55	3.80	0.00200	V	1.36	2.72	2.18	2.72	2.07
				P	-	2.21	2.34	2.34	2.30
				T	2.05	2.05	2.25	2.25	2.14
15	0.60	4.75	0.00240	V	2.72	1.81	1.55	2.18	1.98
				P	-	-	1.70	-	1.70
				T	2.05	1.88	1.73	2.05	1.91
16	0.65	5.57	0.00270	V	1.36	1.21	1.55	1.36	1.36
				P	-	-	-	-	1.36
				T	1.41	1.41	1.61	1.32	1.42
17	0.55	3.74	0.00197	V	1.81	1.81	2.18	2.72	2.07
				P	-	1.97	2.50	-	2.21
				T	2.05	2.25	2.81	1.73	2.14
18	0.60	5.19	0.00262	V	1.81	1.55	1.81	1.55	1.67
				P	0.21	2.08	1.70	1.50	1.73
				T	-	-	-	-	-
19	0.65	5.12	0.00249	V	1.81	1.09	1.36	0.99	1.24
				P	1.25	1.44	1.14	1.29	1.27
				T	1.73	1.41	1.18	1.32	1.38
20	0.65	5.38	0.00234	V	1.55	0.99	1.36	1.21	1.24
				P	0.25	1.21	1.25	1.29	1.25
				T	1.25	1.25	1.41	1.02	1.22

Continued on next page.

Post processing image systems

Digital video camera

The digital video camera, which was used to measure the front velocity, is a JVC GZ-E205. This basic video camera is able to record Full HD video with a frame rate of 1/29 s (29 fps; fps = frames per second), about four times less precise than the photoelectric system. This instrument was used to identify an alternative and cheaper solution than thermo camera. Figure 3 shows the frames (crop of the original images) recorded during a test, evidencing the passage of the front over the marker line (end of the R_1 reach).

Thermo camera

Infrared images were obtained by means of the thermo-camera NEC compact thermo 200ex. The detection system is a camera sensitive to infrared radiation, which shows a false colour image as a function of the temperature of the exposed surface. The temperature range is between -20°C and 500°C with an accuracy of 2°C. The frames were collected every 1/60 s (60 fps), almost the half of the photoelectric-system precision. The thermo camera is able to follow the motion of the debris-flow front as much as video camera does (Figure 4B). In order to capture the dynamics of single particles inside the debris-flow matrix, three particles were previously heated (around 180°C) for each test and then easily added to the mixture. All sizes of the particles were coarser than the 95% of the sieve diameter of the grain-size distribution of the debris-flow mixture under test (diameter greater than 12 mm). The largest dimension of the heated particles was selected to track at the best their paths within the flow and because smaller particles cool down quickly when mixed with the surrounding debris-flow sample. Figure 4 shows the comparison between a frame recorded by

Table 2. Continued from previous page.

Test ID	C_V	M (kg)	V_0 (m^3)	Method of measure	V_1 (m s^{-1})	V_2 (m s^{-1})	V_3 (m s^{-1})	V_4 (m s^{-1})	V_m (m s^{-1})
21	0.55	4.91	0.00211	V	2.18	1.55	2.18	1.55	1.81
				P	2.08	1.79	2.21	-	1.97
				T	2.25	1.73	2.05	1.73	1.91
22	0.60	4.29	0.00261	V	1.55	1.36	2.72	1.81	1.74
				P	1.34	2.08	1.17	7.50	1.81
				T	1.50	1.61	2.05	1.73	1.70
23	0.50	2.16	0.00259	V	2.72	1.55	2.18	2.18	2.07
				P	1.70	2.21	1.14	-	2.05
				T	3.21	1.88	2.50	1.61	2.14
24	0.50	3.54	0.00217	V	2.18	1.81	2.18	2.18	2.07
				P	-	3.75	1.44	5.36	2.62
				T	3.21	1.88	2.25	2.05	2.25
25	0.55	4.18	0.00119	V	2.18	1.81	2.18	2.18	2.07
				P	-	0.13	1.79	-	1.79
				T	1.73	1.88	2.25	2.05	1.96
26	0.60	3.60	0.00195	V	1.21	1.55	1.55	1.55	1.45
				P	-	-	-	-	1.50
				T	1.32	1.18	1.88	1.32	1.38
27	0.65	5.43	0.00220	V	1.09	1.36	1.21	1.36	1.24
				P	-	-	0.91	1.56	1.30
				T	1.32	1.25	1.50	0.98	1.23
28	0.50	4.25	0.00182	V	1.55	2.18	1.55	1.55	1.67
				P	-	0.17	1.34	3.13	1.88
				T	-	-	-	-	-
29	0.50	3.83	0.00263	V	1.55	1.55	1.81	2.72	1.81
				P	-	2.34	2.34	2.88	2.50
				T	3.21	1.18	2.25	2.25	1.96

C_V is the solid concentration by volume of the debris-flow mixture; M and V_0 are the mass and the volume of the mixture arrived to the deposition area, respectively; the symbols indicate: Method of measure: V = video camera, P = photocells, T = thermo camera; V_1, V_2, V_3 and V_4 are the mean velocities of the front recorded by the three instruments in the reaches R_1, R_2, R_3 and R_4; V_m is the mean velocity of the front between the *Start* photocell and the flume end.

Table 3. Average (μ), standard deviation (σ), and coefficient of variation (σ*) of the velocities (V_i) collected by the three instruments in the different sections (P_i) and in the reach from *Start* to P_4 (V_m), and P-values of the Friedman's related samples test.

V_i code	N. of test compared	Photocells			Thermo camera			Video camera			P-value
		μ (m s^{-1})	σ (m s^{-1})	σ^* (-)	μ (m s^{-1})	σ (m s^{-1})	σ^* (-)	μ (m s^{-1})	σ (m s^{-1})	σ^* (-)	
V_1	9	1.41	0.51	0.36	1.76	0.61	0.35	1.79	0.42	0.23	0.016*
V_2	18	1.79	0.73	0.41	1.53	0.35	0.23	1.52	0.44	0.29	0.002*
V_3	20	1.69	0.52	0.31	1.89	0.46	0.24	1.93	0.50	0.26	0.287
V_4	12	1.62	0.57	0.35	1.48	0.46	0.31	1.67	0.61	0.37	0.264
V_m	23	1.73	0.42	0.24	1.66	0.34	0.20	1.67	0.33	0.20	0.587

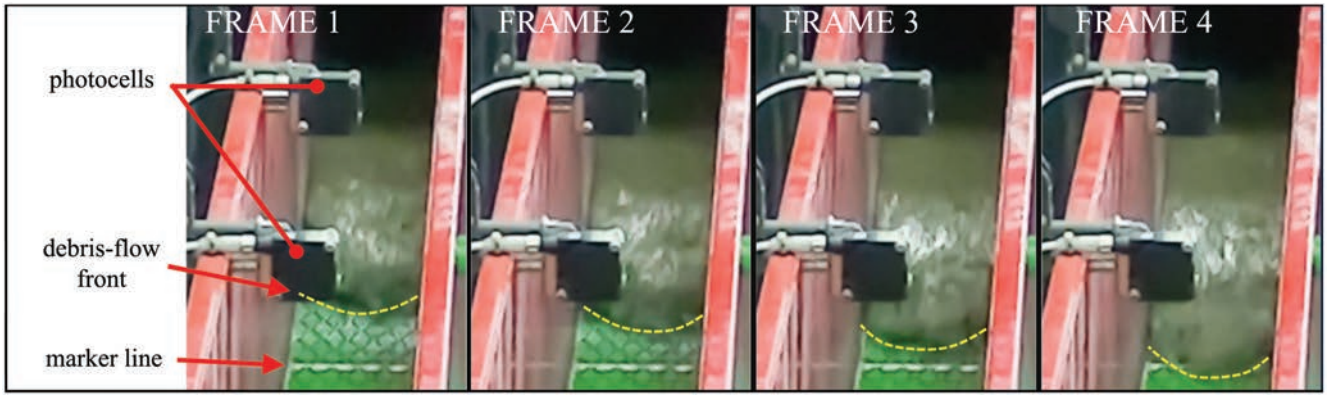

Figure 3. Frame sequence recorded by the digital video camera of a laboratory test (ID 27 in Table 2): transit of the front on the reference line at the end of the reach 1.

the video camera and the corresponding one provided by the thermo camera. In the second frame the heated particles stand out clearly from the rest of debris-flow matrix.

Results

A total of 29 laboratory tests were performed using mixtures with different sediment concentration. The bulked volumes of the debris-flow material arriving to the depositional area range from 30% to 80% of the total released material (4000 cm^3). The whole experimental dataset is listed in Table 2.

The flow-front transit was detected in the 4 control sections ($P_{1\text{-}4}$) and then the related velocities ($V_{1\text{-}4}$) and the mean flow velocities were calculated as described in the previous section (V_m). Hence, a total of 145 velocity data were collected for each device. Due to the characteristics of the detection systems, some velocities were not recorded: 35 for photocells, 15 for video camera, and 20 for thermo camera (Table 2). Therefore, the total number of the velocities detected in each control section was: 64 for V_1 in the R_1 reach, 74 for V_2 in R_2, 77 for V_3 in R_3, 70 for V_4 in R_4, and 80 for V_m (Figure 5). The variability of the values of recorded data for each V_i section is mainly caused by different C_V. V_1 ranges from 0.21 to 3.21 m/s (mean value 1.69 m/s), V_2 ranges from 0.13 to 3.75 m/s (mean value 1.58 m/s), V_3 ranges from 0.91 to 2.81 m/s (mean value 1.81 m/s), V_4 ranges from 0.98 to 3.13 m/s (mean value 1.75 m/s) and V_m ranges from 1.15 to 2.62 m/s (mean value 1.69 m/s).

A Friedman's related samples test was used to compare the velocities measured by photocells, video camera, and thermo camera. The P-value <0.05 level was used to determine the statistical significance. The statistical test was applied to the velocities recorded in the different sections P_i, using only each laboratory run during which the all three instruments have been operating; 9 laboratory tests were used to compare V_1 collected by the three methods, 18 tests for V_2, 20 tests for V_3, 14 tests for V_4, and 23 tests for V_m. The results of the statistical analysis are reported in Table 3 that shows the average (μ), the standard deviation (σ), and the coefficient of variation (σ^*) of the front velocity recorded with the three devices in the different sub-reaches and also it reports the P-value of the test. The values of the coefficient of variation (σ^*) indicate a low variance of the gauged velocities for the image analysis devices, whereas greater variability (σ^* ranges from 0.24 to 0.41) was observed for the photocells, in particular in the recording section P_4, channel end ($\sigma^* = 0.41$).

Figure 6 provides a representation of the recorded mean velocities. The analysis (Table 3) indicates statistically significant differences in the reaches R_1 and R_2, which are placed in the first part of the flume.

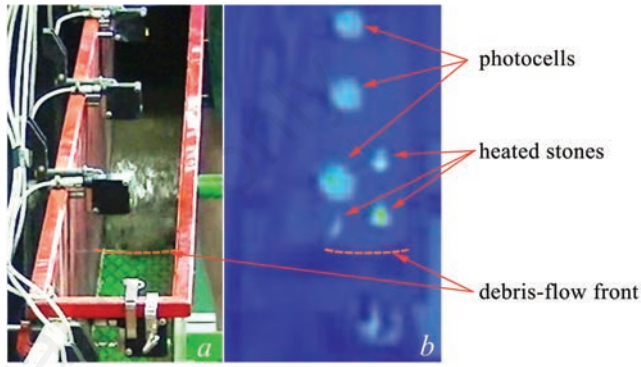

Figure 4. Comparison between a frame recorded by the video camera (A) and the corresponding one recorded by the thermo camera (B), during the test n. 27 of Table 2; the frame collected by the thermo camera allows the identification of the heated particles (photocells are also visible because they are heated by the passage of an electric current).

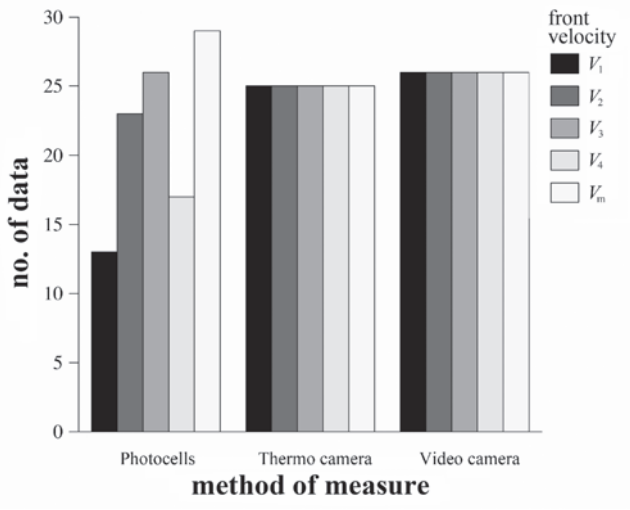

Figure 5. The number of data collected for each velocity from the three different measuring devices.

For the second part of the flume (reaches R_3 and R_4) as well as for the mean velocity in the entire channel, the three instruments seem to provide comparable values of velocity. A multiple comparison procedure, using the same statistical tests, was adopted to determine which instrument provides velocities significantly different from the others in R_1 and R_2. The analysis states that video camera and thermo camera provide not significantly different velocities, while photocells differ statistically (P-value of the Friedman tests <0.05) from the other two instruments.

The velocity data obtained by the video camera were used to analyse the influence of the solid concentration C_V of the mixture on the velocity along the flume (Figure 7). Video camera was chosen because of the greater number of sampled data with respect to data measured with the other instruments. Our small-scale simulations prove the front velocity reduces with increasing C_V (Figure 7) and this reduction is remarkable passing from C_V = 0.50-0.55 to C_V = 0.60-0.65. Table 4 summarizes the average (μ), the standard deviation (σ), and the coefficient of variation (σ^*) of the front velocity recorded in the different reaches for mixtures having same volumetric concentration. The σ^* values range from 0.03 to 0.28 and indicate a low variance of the gauged velocities. Kruskal-Wallis test was then conducted to compare the mean velocities in the same sub-reach for different C_V classes. A P-value of <0.05 was considered to be statistically significant. The comparison of the four means using Kruskal-Wallis test (Table 4) points out a statistically significant difference in the velocity in each section except in R_1.

Finally, the images obtained with the thermo camera were used to investigate the behaviour of single particles during the motion. The particles movement was tracked manually through the frame analysis. The data of the particles slowed by collisions against the flume walls were excluded from the database, therefore the 36 heated particles analysed ranges from 12.0 mm to 19.0 mm: 8 in the first quartile (diameters from 12.0 mm to 13.5 mm), 9 in the second quartile (diameters from 13.8 mm to 14.4 mm), 9 in the third quartile (diameters from 14.4 mm to 15.5 mm), and 10 in the fourth quartile (diameters from 15.6 mm to 19.0 mm). The velocities of these particles were compared with the front velocities. The average velocities of the particles for the four solid concentrations decrease as the C_V increases. The same behaviour occurs for the velocities of the debris-flow front. The analysis of the particle sizes indicates that the largest ones (the fourth quartile of the heated particles) were more easily stopped due to frictions with the flume bottom and dissipative collisions against the flume walls (more than 50% belonging to the fourth quartile). Differently, less than 25% of the particles belonging to the first finest-size quartile were stopped. No correlation was observed between the particles size and their mean velocity for those particles reaching the depositional plain (coefficient of determination R^2 = 0.11).

Table 5 shows the slope m, the intercept q and the coefficient of determination R^2 of the linear regression - general form $V_s = m\ V_m + q$ - between the front velocity and the particle velocity, respectively V_m and V_s, for each quartile of the particles size. The R^2 value remains always in the range 0.6-0.8. It can be noted that the particles belonging to the first quartile seem to be more reactive to front velocity variations, as indicated by the high inclination of linear regression (Table 5) and by the trend depicted in Figure 8.

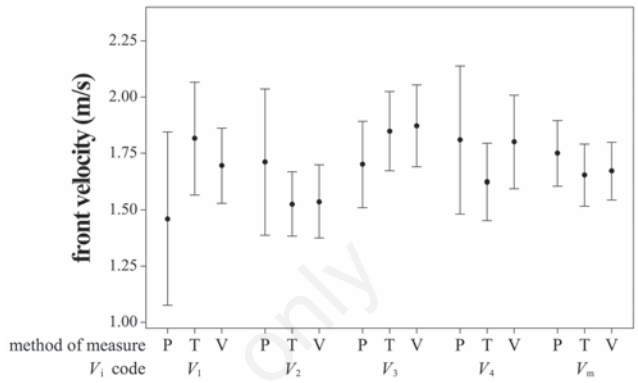

Figure 6. Means and 95% confidence intervals for the means of the velocity V_i; P = photocells; T = thermo camera; V = video camera.

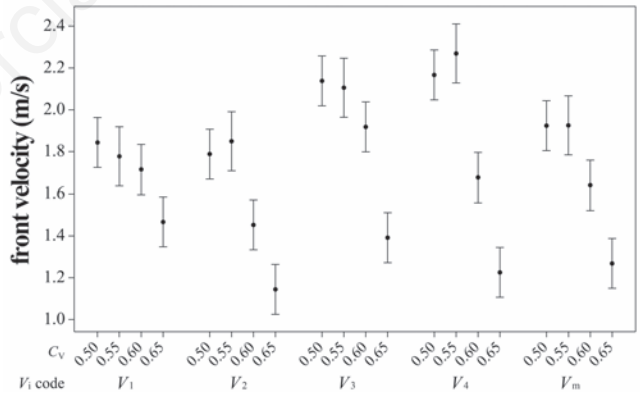

Figure 7. Plot of the means (± standard error bars) of the V_i velocity (video camera data) and associated volumetric concentration C_V.

Table 4. Average (μ), standard deviation (σ), and coefficient of variation (σ*) of the velocities collected in the different sections (velocity V_i) and in the reach from *Start* to P_4 (V_m), for the four C_V, and P-values of the Kruskal-Wallis test.

V_i code	C_V = 0.50			C_V = 0.55			C_V = 0.60			C_V = 0.65			P-value
	μ (m s^{-1})	σ (m s^{-1})	σ^* (-)	μ (m s^{-1})	σ (m s^{-1})	σ^* (-)	μ (m s^{-1})	σ (m s^{-1})	σ^* (-)	μ (m s^{-1})	σ (m s^{-1})	σ^* (-)	
V_1	1.84	0.45	0.24	1.78	0.41	0.23	1.72	0.49	0.28	1.47	0.22	0.15	0.328
V_2	1.78	0.21	0.12	1.85	0.52	0.28	1.45	0.25	0.17	1.14	0.17	0.15	0.001
V_3	2.14	0.45	0.21	2.11	0.17	0.08	1.92	0.41	0.21	1.39	0.23	0.17	0.004
V_4	2.16	0.34	0.16	2.27	0.48	0.21	1.68	0.24	0.14	1.23	0.15	0.12	<0.001
V_m	1.92	0.15	0.08	1.93	0.20	0.10	1.64	0.20	0.12	1.27	0.04	0.03	<0.001

Discussion

The comparative analysis between different methods to measure the debris-flow velocity in the field is a research topic already considered and discussed by different authors (*e.g.*, Arattano and Marchi, 2005). To the opposite, specific studies comparing alternative methods for small-scale experiments are lacking. Our experiments compare two standard methods - photocells and video camera - to measure the front velocity for miniature debris flows and it considers, in addition, the promising technique of the high-speed thermo camera, which is innovative in this research field. The results highlight that the velocity measured by the three instruments is statistically different in the first part of the flume, but not in the second. One possible explanation is that the surge formation in the upper part of the flume makes the direct measurements with the photocells more prone to delay the front-passage detection (Figure 6) because the front thickness was too small (<5 mm), being under formation.

The statistical analysis shows that velocity values obtained with the laser photoelectric sensor system differ from those obtained by other systems. The thermo camera and the video camera, in fact, provide comparable velocity values (Table 3 and Figure 6). Differences can be ascribed to the technique of the laser photoelectric sensor system in velocity measurement, because the photoelectric sensors are highly sensitive and could be activated not only by the passage of the front, but also by mud splashes, flume vibrations or single particles that overrun the front, particularly in the final sub-reach (velocity V_4, Figure 6). Moreover, the vibrations of the flume sometimes activated the photoelectric sensors before the passage of the front in the *Start* section (Figure 1) and fully endangered the data collection. As a consequence, an important condition to achieve an accurate velocity measurement with a laser photoelectric system is a stable flume. Such a restriction does not occur in using video camera and thermo camera since the motion is verified through the image post-process analysis.

Lack of data in the thermo camera and video camera gauging depends on missing recordings, in other words it depends on human errors. In particular, the thermo camera can record 400 real time frames. The maximum recording time, setting a speed of 60 fps, is equal to 6.67 s. This means that the recording has to start approximately at the moment of the gate opening, but the manual operation can cause an anticipated recording and then a lack of data for the whole test.

Focusing on the sediment concentration C_V, this was confirmed to strongly affect the debris-flow motion as showed by different Authors (Zhou *et al.*, 1999; Ancey, 2001; Ancey, 2007). In comparison with C_V = 0.50, the velocity reduction is equal to 20% for C_V = 0.60 and 36% for C_V = 0.65 (Figure 9). This slowdown is probably associated with a transition from an inertial regime to a macroviscous regime, as already shown by Bettella *et al.* (2012) experiments.

Dealing with the particles dynamics inside the mixture, previous researchers (Takahashi, 1980; Iverson, 1997; Yamagishi *et al.*, 2003) recognized that boulders within a debris flow tend to be faster and accumulate at the flow front. Takahashi (1980) applied Bagnold's (1954) dispersive pressure to his model to explain the upward motion of a large particle in a grain flow. These all findings are confirmed by our laboratory observations that quantitatively indicate the same behaviour (Figure 8) also at a small-scale. The particles inside the debris-flow front exhibited higher mean velocities (from *Start* to P_4 in Figure 1) than the front velocity (Figure 8). In fact, we registered a velocity increment for the particle equal to 13% on average. It is worth noting that particles with diameter of the order of debris-flow depth show a double behavior: a fraction (less than 50%) arrived at the depositional plane travelling slightly faster than the front velocity, the other fraction stopped during the motion due to the

Table 5. Slope *m*, intercept *q* and coefficient of determination R^2 of the linear regression between front and particle velocities for each quartile of the particles size.

Quartile	*m*	*q*	R^2
I	1.4738	-0.5072	0.79
II	0.9736	0.2807	0.65
III	0.9127	0.4473	0.57
IV	1.1417	0.0672	0.80
Total	1.0876	0.1168	0.71
II-III-IV	1.0078	0.2684	0.67

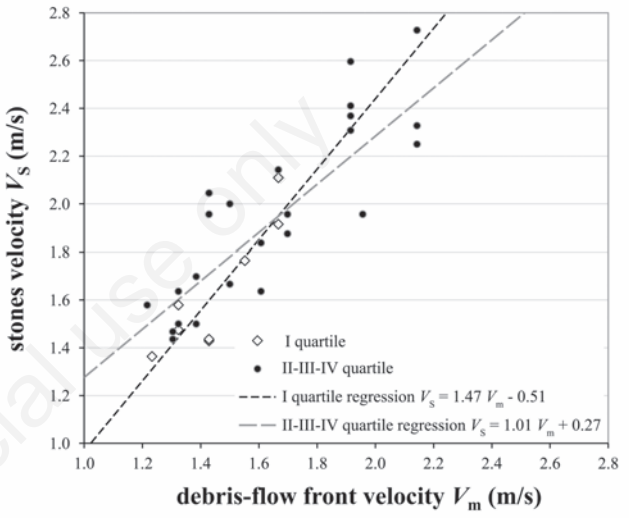

Figure 8. Debris-flow front velocities V_m (image post-processing) against heated-particles velocities V_S (thermo camera).

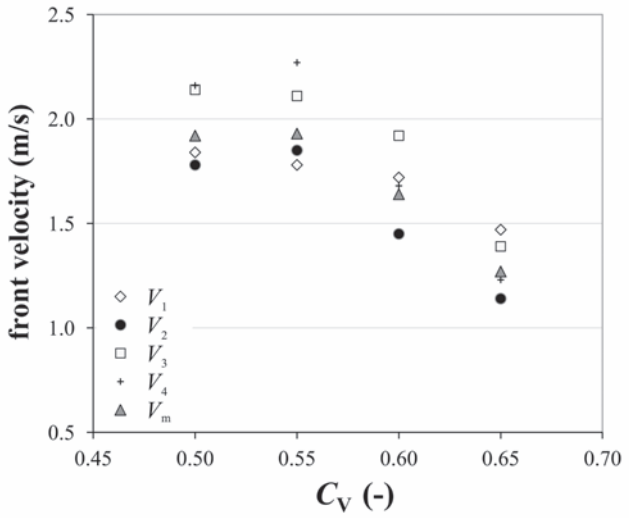

Figure 9. Average front velocity (V_i and V_m) against the solid concentration C_V.

friction with the flume perimeter. In conclusion, according to Prochaska *et al.* (2008), our laboratory debris flows entrained both boulders - the smallest - travelling just faster the maximum surface velocity and boulders - the coarsest - having slightly slower velocities because they mainly slid and rolled (Iverson, 2003).

Conclusions

The purpose of this research was to compare mean velocity measurements in a small-scale modelling of debris flows through two different methods: a timing system based on laser photoelectric sensors and a post processing images system. This last was achieved using different devices: a normal video camera and a high-speed thermo camera. Both methods measure the time lag between the front passages in two cross-sections, allowing an assessment of the mean velocity within the reach.

The main outcomes can be summarised as follows:

- The laser photoelectric sensors system seems the best option because of high precision (0.01 s in our case) and easy to use. In fact, it provides time data directly and it does not require further time-consuming post-processing as the image-processing does. On the other side, the measurements highlighted some weaknesses, which can complicate its use due to flume vibrations, mud splashes, and single particles passing the front.
- The post processing images system approach is less precise (in our case from 1/29 s to 1/60 s respectively equal to 0.034 s and 0.017 s, depending on the device) and it requires a post-processing of images to calculate the velocity. Our tests proved that this method is more reliable in practice, allowing the collection of a larger amount of data of high quality. The post-processing image operations resulted time consuming, but allowed an accurate analysis of the debris-flow motion and the distinction between front, mud splashes, and single particles is quite clear.
- The choice of the detection device is relevant to define the data accuracy in the following resolutions: frame rate, which affects the time precision, and detail level of the images (image resolution and quality), which supports a clear identification of single portions of the debris-flow wave.
- A non-professional video camera and a more sophisticated thermo camera resulted equivalent in terms of assessing the front velocity.
- The high-speed thermo camera has proven to be capable of tracking the motion of single particles and has opened new research opportunities in the knowledge of debris-flow mechanics through laboratory modelling at small-scale. Further researches could be addressed to automatically track single debris-flow particles from thermo-camera images.

References

Ancey C. 2001. Role of lubricated contacts in concentrated polydisperse suspensions. J. Rheol. N.Y. 1421:1439-45.

Ancey C. 2007. Plasticity and geophysical flows: a review. J. Non Newtonian Fluid Mech. 4:35-145.

Arattano M., Deganutti A.M., Marchi L. 1997. Debris flow monitoring activities in an instrumented watershed on the Italian Alps. In: C.L. Chen (ed.), Proc. First Int. Conf. on Debris-flow hazards mitigation: mechanics, prediction and assessment. ASCE, New York, NY, USA, pp 506-515.

Arattano M., Marchi L. 2000. Video-derived velocity distribution along a debris flow surge. Phys. Chem. Earth Part B. 781:784-25.

Arattano M., Marchi L. 2005. Measurements of debris flow velocity through cross-correlation of instrumentation data. Nat. Hazards Earth Syst. Sci. 137:142-5.

Arattano M., Moia F. 1999. Monitoring the propagation of a debris flow along a torrent. Hydrol. Sci. J. 811:823-44.

Bagnold, R.A. 1954. Experiments on a gravity-free dispersion of large solid spheres in a Newtonian fluid under shear. Proc. Roy. Soc. London. 49:63-A225.

Bettella F., Bisantino T., D'Agostino V., Gentile F. 2012. Debris-flow runout distance: laboratory experiments on the role of Bagnold, Savage and friction numbers. In: D. DE Wrachien, C.A. Brebbia, S. Mambretti (eds.), Monitoring, simulation, prevention and remediation of dense and debris flows IV. WIT Transactions on Engineering Sciences, Vol 73. WIT Press, Southampton, UK, pp 27-36.

Chow V.T. 1959. Open channel hydraulics. McGraw-Hill, Singapore.

Comiti F., Marchi L., Macconi P., Arattano M., Bertoldi G., Borga M., Brandinoni F., Cavalli M., D'Agostino V., Penna D., Theule J. 2014. A new monitoring station for debris flows in the European Alps: first observations in the Gadria basin. Nat. Hazards. 1:24-73.

D'Agostino V., Bettella F., Cesca M. 2013. Basal shear stress of debris flow in the runout phase. Geomorphology. 272:280-201.

Hürlimann M., McArdell W.B., Rickli C. 2015. Field and laboratory analysis of the runout characteristics of hillslope debris flows in Switzerland. Geomorphology. 20:32-232.

Inaba H., Uddin M.S., Itakura Y., Kasahara M. 1997. Surface velocity vector field measurement of debris flow based on spatiotemporal derivative space method. In: C.L. Chen (ed.), Proc. First Int. Conf. on Debris-flow hazards mitigation: mechanics, prediction and assessment. ASCE, New York, NY, USA, pp 757-766 .

Itakura Y., Koga Y., Takahama J., Nowa Y. 1997. Acoustic detection sensor for debris flow. C.L. Chen (ed.), Proc. First Int. Conf. on Debris-flow hazards mitigation: mechanics, prediction and assessment. ASCE, New York, NY, USA, pp 747-756.

Itakura Y., Ogawa K., Suwa H., Mizuhara K. 1985. Trends and fluctuation of the surface-velocity of debris flow measured by a non-contact speed sensor with a spatial filter. In: M. Harada (ed.), Fluid control and measurement. Pergamon Press, Tokyo, Japan, pp 781-786.

Itakura Y., Suwa H. 1989. Measurement of surface velocity of debris flows by spatial filtering velocimetry. pp 199-203 in Proc. Japan China Symp. on Landslides and debris flows, Niigata, Tokyo, Japan.

Iverson R.M. 1997. The physics of debris flows. Rev. Geophy. 245:296-35.

Iverson R.M. 2003. The debris-flow rheology myth. In: D. Rickenmann and C.L. Chen (eds.), Debris-flow hazard mitigation: mechanics, prediction, and assessment - Proc. 3rd Int. Conf. Mills Press, Rotterdam, Netherlands, pp 303-314.

Iverson R.M., Logan M., LaHusen R.G., Berti M. 2010. The perfect debris flow? Aggregated results from 28 large-scale experiments. J. Geophys. Res. 115:F03005.

Larcher M., Fraccarollo L., Armanini A., Capart H. 2007. Set of measurement data from flume experiments on steady uniform debris flows. J. Hydraul. Res. 59:71-45.

Pierson T.C. 1986. Flow behavior of channelized debris flows, Mount St. Helens, Washington. In: A.D. Abrahms (ed.), Hillslope processes. Allen & Unwin, Boston, MA, USA, pp 269-296.

Prochaska A.B., Santi P.M., Higgins J.D. 2008. Relationships between size and velocity for particles within debris flows. Can. Geotechn. J. 1778:1783-45.

Suwa H., Okunishi K., Sakai M. 1993. Motion, debris size and scale of debris flows in a valley on Mount Yajkedake, Japan. In: R.F. Hadley and T. Mizuyama (eds.), Sediment problems: strategies for monitoring, prediction and control - Proc. Yokohama Symp., July 1993. IAHS Publ. No. 217. IAHS, CEH, Wallingford, UK, pp 239-248.

Takahashi T. 1980. Debris flow in prismatic open channel. J. Hydraul.

Div. ASCE. 381:396-106.
Tuyen N.B., Cheng N.S. 2012. A single-camera technique for simultaneous measurement of large solid particles transported in rapid shallow channel flows. Exp. Fluids. 1269:1287-53.
Yamagishi M., Mizuyama T., Satofuka Y., Mizuno H. 2003. Behavior of big boulders in debris flow containing sand and gravel. In: D. Rickenmann and C.L. Chen (eds.), Debris-flow hazard mitigation: mechanics, prediction, and assessment - Proc. 3rd Int. Conf. Mills Press, Rotterdam, Netherlands, pp 411-420.
Zhou Z., Solomon M.J., Scales P.J., Boger D.V. 1999. The yield stress of concentrated flocculated suspensions of size distributed particles. J. Rheol. 651:671-43.